J. Fluid Mech. (1974), *vol.* 65, *part* 1, *pp.* 177–188
Printed in Great Britain

Reynolds-shear-stress measurements in a compressible boundary layer within a shock-wave-induced adverse pressure gradient

By W. C. ROSE

Ames Research Center, NASA, Moffett Field, California 94035

AND M. E. CHILDS

University of Washington, Seattle, Washington 98195

(Received 11 July 1973)

The results of an experimental investigation of the mean- and fluctuating-flow properties of a compressible turbulent boundary layer in a shock-wave-induced adverse pressure gradient are presented. The turbulent boundary layer developed on the wall of an axially symmetric nozzle and test section whose nominal free-stream Mach number and boundary-layer-thickness Reynolds number were 4 and 10^5, respectively. The adverse pressure gradient was induced by an externally generated, conical shock wave.

Mean and time-averaged fluctuating-flow data, including the experimental Reynolds shear stresses and experimental turbulent heat-transfer rates, are presented for the boundary layer and external flow, upstream, within and downstream of the pressure gradient. The turbulent mixing properties of the flow were determined experimentally with a hot-wire anemometer. The calibration of the wires and the interpretation of the data are discussed.

From the results of the investigation, it is concluded that the shock-wave/boundary-layer interaction significantly alters the shear-stress characteristics of the boundary layer.

1. Introduction

The behaviour of compressible turbulent boundary layers in strong adverse pressure gradients, particularly those gradients induced by oblique shock waves in supersonic flows, is of prime current interest. One major source of this interest is the desire to predict the behaviour of a turbulent boundary layer in both internal and external aerodynamic flows on aircraft that are to fly at supersonic and hypersonic Mach numbers. Shock waves are always present at these Mach numbers; generally, when they interact with the boundary layer (whether in an internal flow such as the engine inlet system or an external flow such as a deflected control surface), a strong retarding (adverse) pressure gradient acts on the boundary layer. This gradient causes a modification of the boundary layer itself, as well as of the flow outside the boundary layer. The modifications to the boundary-layer flow through the shock-wave/boundary-layer interaction

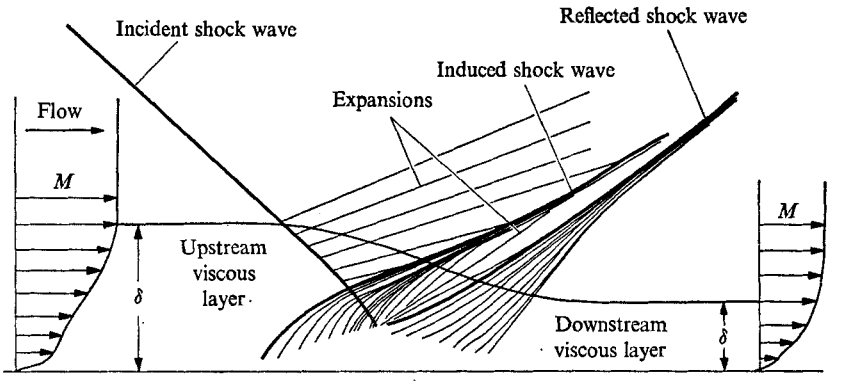

FIGURE 1. Schematic diagram of shock-wave/boundary-layer interaction region. δ is the boundary-layer thickness and M the Mach number.

region (figure 1) include changes in mean profile shape (possibly including separation) and changes in the turbulent mixing properties of the layer.

A primary goal of fluid mechanics research today is to develop computing techniques which take advantage of recent developments in computer hardware to predict the behaviour of boundary layers in interaction regions. If these computing techniques are to provide realistic solutions for interaction phenomena, a basic understanding of such phenomena (e.g. turbulent transport rates) is required. The interaction phenomena may be broadly divided into two categories denoted here by 'mean' and 'fluctuating'. The mean quantities, such as velocity profiles, shock-wave locations and the extent of separated regions, are the ones most frequently studied. The fluctuating quantities, which are those related to turbulent mixing rates, have been investigated to a much lesser extent, in spite of their important role in determining the mean quantities. A brief review of results of some of the past investigations of fluctuating flow is given below.

Kistler (1959) reported distributions of $\langle(\rho u)'\rangle$, $\langle T_t'\rangle$ and $\overline{(\rho u)' T_t'}$ across a zero-pressure-gradient turbulent boundary layer at Mach numbers of 1·71, 3·56 and 4·67 for a single streamwise location, where ρ is the density, u the streamwise velocity, T_t the total temperature, a prime denotes a fluctuating quantity, an overbar a time-averaged quantity and angular brackets an r.m.s. value. Laufer (1961) measured the mass flux and total-temperature fluctuations outside a zero-pressure-gradient turbulent boundary layer and concluded that they were produced solely by pressure fluctuations radiated from it. These two investigations were carried out using hot-wire anemometers. However, none of the measurements was converted to a form that could be used to assess relative magnitudes of the turbulent stresses, such as $\overline{\rho}\,\overline{u'^2}$ or $\overline{u}\,\overline{\rho' u'}$, in the momentum equations. Morkovin & Phinney (1958) considered the use of a yawed wire to determine the $\overline{v'^2}$-like fluctuations, the shear-stress-like term $\overline{u'v'}$ and the heat-transfer-like term $\overline{v'T'}$. They present the shear-stress and heat-transfer measurements at one location in a zero-pressure-gradient turbulent boundary layer.

The purpose of the present investigation was to obtain mean- and fluctuating-flow data, including the Reynolds shear stress and turbulent heat-transfer rates, upstream, within and downstream of a shock-wave/boundary-layer interaction.

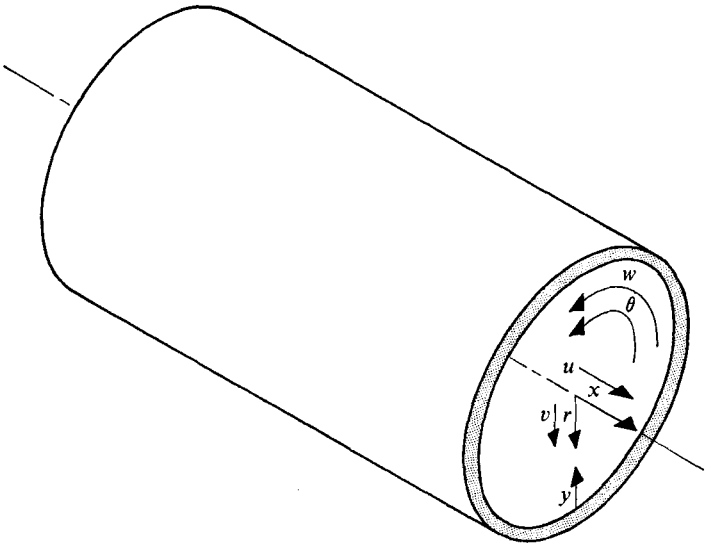

FIGURE 2. Nomenclature for co-ordinate and velocity components. x is measured from the tip of the conical shock-wave generator (see figure 3).

2. Conservation equations

The time-averaged conservation equations for mass, momentum and thermal energy for axially symmetric flow (see figure 2 for co-ordinate system) may be written, after a complete Reynolds decomposition of the flow variables into mean and fluctuating components, as

$$\frac{\partial \overline{\rho u}}{\partial x}+\frac{1}{r}\frac{\partial r\overline{\rho v}}{\partial r}+\frac{\partial \overline{\rho' u'}}{\partial x}+\frac{1}{r}\frac{\partial r\overline{\rho' v'}}{\partial r}=0 \quad \text{(continuity)}, \tag{1}$$

$$\frac{\partial \overline{\rho u}\,\overline{u}}{\partial x}+\frac{1}{r}\frac{\partial r\overline{\rho u}\,\overline{v}}{\partial r}=-\frac{\partial \overline{p}}{\partial x}+\frac{\partial}{\partial x}[\overline{\tau_{xx}}-(\overline{\rho u'u'}+2\overline{u}\,\overline{\rho' u'})]$$
$$+\frac{1}{r}\frac{\partial}{\partial r}r[\overline{\tau_{rx}}-(\overline{\rho u'v'}+\overline{u}\,\overline{\rho' v'}+\overline{v}\,\overline{\rho' u'})] \quad (x \text{ momentum}), \tag{2a}$$

$$\frac{\partial \overline{\rho u}\,\overline{v}}{\partial x}+\frac{1}{r}\frac{\partial r\overline{\rho v}\,\overline{v}}{\partial r}=-\frac{\partial \overline{p}}{\partial r}-\frac{1}{r}(\overline{\tau_{\theta\theta}}-\overline{\rho w'w'})+\frac{\partial}{\partial x}[\overline{\tau_{xr}}-(\overline{\rho u'v'}+\overline{u}\,\overline{\rho' v'}+\overline{v}\,\overline{\rho' u'})]$$
$$+\frac{1}{r}\frac{\partial}{\partial r}r[\overline{\tau_{rr}}-(\overline{\rho v'v'}+2\overline{v}\,\overline{\rho' v'})] \quad (r \text{ momentum}), \tag{2b}$$

$$0=\frac{\partial}{\partial x}[\overline{\tau_{x\theta}}-(\overline{\rho u'w'}+\overline{u}\,\overline{\rho' w'})]+\frac{1}{r^2}\frac{\partial}{\partial r}r^2[\overline{\tau_{r\theta}}-(\overline{\rho v'w'}+\overline{v}\,\overline{\rho' w'})] \quad (\theta \text{ momentum}), \tag{2c}$$

$$\frac{\partial \overline{\rho u}\,\overline{h}}{\partial x}+\frac{1}{r}\frac{\partial r\overline{\rho v}\,\overline{h}}{\partial r}=\overline{u}\frac{\partial \overline{p}}{\partial x}+\overline{v}\frac{\partial \overline{p}}{\partial r}+\overline{u'\frac{\partial p'}{\partial x}}+\overline{v'\frac{\partial p'}{\partial r}}+\overline{\mu\phi}$$
$$+\frac{\partial}{\partial x}\left[\overline{k\frac{\partial T}{\partial x}}-(\overline{\rho u'h'}+\overline{u}\,\overline{\rho' h'}+\overline{h}\,\overline{\rho' u'})\right]$$
$$+\frac{1}{r}\frac{\partial}{\partial r}r\left[\overline{k\frac{\partial T}{\partial r}}-(\overline{\rho v'h'}+\overline{v}\,\overline{\rho' h'}+\overline{h}\,\overline{\rho' v'})\right] \quad \text{(energy)}, \tag{3}$$

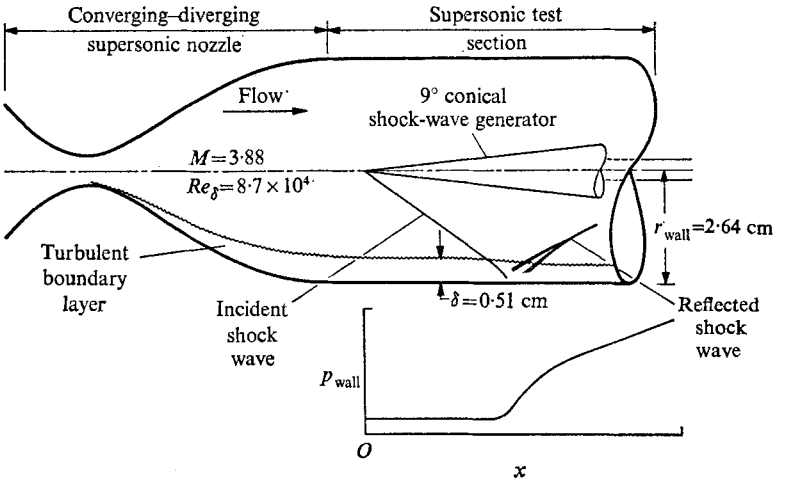

FIGURE 3. Schematic diagram of experimental facility.

where k is the thermal conductivity, μ the absolute viscosity, h the enthalpy per unit mass and $\mu\phi$ the dissipation per unit volume. The equation of state is

$$\overline{p} = R(\overline{\rho}\,\overline{T} + \overline{\rho' T'}). \tag{4}$$

Generally, in boundary-layer studies, the turbulent shear-stress term $\overline{\rho u' v'}$ in (2a) and the turbulent heat-transfer term $\overline{\rho v' h'}$ in (3) (or $c_p \overline{\rho v' T'}$) are of prime concern. These are usually further simplified to $\overline{\rho}\,\overline{u'v'}$ and $c_p \overline{\rho}\,\overline{v'T'}$ by neglecting the triple correlations.

In the present study, experimental values of $\overline{\rho}\,\overline{u'v'}$ and $\overline{\rho}\,\overline{u'T'}$ are presented for various streamwise locations throughout a region of interaction between a shock wave and a turbulent boundary layer. These measured values are discussed in the light of possible mathematical models of the turbulent transport terms.

3. Experimental investigation

The experimental investigation was conducted in an axially symmetric flow facility to minimize three-dimensional effects. Figure 3 is a schematic diagram of the experimental arrangement used in the investigation. A complete description of the experimental apparatus is given by Rose (1972).

The Mach number M for the core flow in the test section was 3·88 ± 0·02. The Reynolds number Re_δ based on the thickness of the undisturbed boundary layer was $8{\cdot}7 \times 10^4$. The total temperature in the free stream was 300 °K, and the wall temperature was near the adiabatic wall temperature for the test-section Mach number. The total pressure ahead of the incident shock wave was $3{\cdot}7 \times 10^5$ N/m².

The measurements were taken in the turbulent boundary layer on the wall of the circular test section. The adverse pressure gradient was imposed on the boundary layer by a conical shock wave generated by a 9° half-angle cone placed

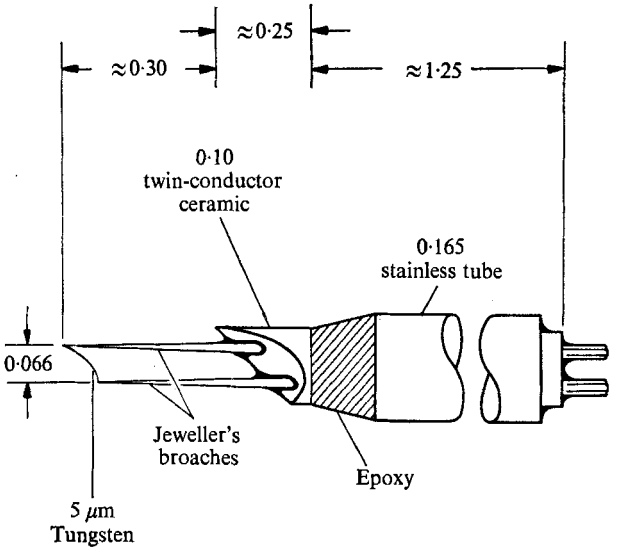

FIGURE 4. Hot-wire probe. All dimensions except wire diameter in cm.

in the centre of the test section. The shock strength for this cone was near that required for separation of the boundary layer. This experimental arrangement produced a steep pressure rise in the immediate region of the interaction followed by an almost linear, but shallower pressure rise in the downstream flow. Mean- and fluctuating-flow data were taken throughout these regions of pressure rise.

3.1. *Instrumentation*

The mean-flow data consist of Pitot pressures, wall surface static pressures and total temperatures. The Pitot pressures were obtained with a flattened miniature Pitot probe, and the total temperatures were obtained by using a hot wire as a resistance thermometer. Static pressures in the flow field were not measured but were calculated from the method given by Rose (1970). The fluctuating-flow data consist of the turbulent transport terms $\overline{\rho}\,\overline{u'v'}$ and $\overline{\rho}\,\overline{v'T'}$. These terms were obtained by using a DISA Model 55D01 constant-temperature hot-wire anemometer. A yawed wire (of the type shown in figure 4, with a yaw angle of approximately 45°) was used as the sensor. The wire itself was 5 μm tungsten. The combined probe and anemometer system gave an upper frequency response high enough to resolve disturbances greater than $\frac{1}{5}\delta$ in the outer part of the boundary layer and $\frac{1}{8}\delta$ in the lower part (Rose 1972).

3.2. *Hot-wire signal interpretation*

On the basis of the work of Morkovin & Phinney (1958), it may be shown that a yawed wire in a supersonic stream for which $M \sin\phi > 1{\cdot}2$, where ϕ is the angle of the wire relative to the local flow, produces a fluctuating voltage response to fluctuating physical variables which may be expressed as

$$E' = \Delta e_{T_t}\left(100\frac{T_t'}{\overline{T}_t}\right) + \Delta e_{\rho u}\left(100\frac{(\rho u)'}{\overline{\rho u}}\right) \pm \Delta e_v\left(100\frac{v'}{\overline{u}}\right). \tag{5}$$

The quantities $\Delta e_{()}$ are the fluctuation sensitivities to the respective physical variables. They have the form (following Morkovin & Phinney 1958)

$$\Delta e_{\rho u} = \frac{\bar{E}}{200}\left[\frac{\partial \ln Nu_t}{\partial \ln Re_t} - \frac{1}{\tau_{wr}}\frac{\partial \ln \eta}{\partial \ln Re_t}\right], \tag{6a}$$

$$\Delta e_{T_t} = \frac{\bar{E}}{200}\left[n_t + 1 - \left\{\frac{\partial \ln Nu_t}{\partial \ln \theta} + \frac{\theta}{\theta - \eta}\right\}\right] - m_t(\Delta e_{\rho u}), \tag{6b}$$

$$\Delta e_v = \frac{\bar{E}}{200}\left[\frac{1}{\tau_{wr}}\frac{\partial \ln \eta}{\partial \phi} - \frac{\partial \ln Nu_t}{\partial \phi}\right], \tag{6c}$$

where

$$n_t = \partial \ln k_t / \partial \ln T_t, \quad m_t = \partial \ln \mu_t / \partial \ln T_t,$$

$$\eta = T_r/T_t, \quad \theta = T_w/T_t, \quad \tau_{wr} = (T_w - T_r)/T_r,$$

Nu and Re are the Nusselt and Reynolds numbers and the subscripts r, w and t (here and elsewhere) denote recovery, wire and total conditions respectively.

As noted by Rose (1972), a form of the sensitivities which is convenient for direct calibration of the hot wire may be obtained directly from (5) as

$$\Delta e_{T_t} = \frac{\bar{E}}{100}\frac{\partial \ln E}{\partial \ln T_t}, \quad \Delta e_{\rho u} = \frac{\bar{E}}{100}\frac{\partial \ln E}{\partial \ln \rho u}, \quad \Delta e_v = \frac{\bar{E}}{100}\frac{\partial \ln E}{\partial \phi}. \tag{7}$$

The sensitivities in (7) were determined for each wire as follows. The value of $\partial \ln E/\partial \ln(\rho u)$ was obtained from the slope of a logarithmic plot of E *vs.* ρu for the range of Reynolds and Mach numbers encountered in the boundary layer. The wire was mounted on the centre-line of the tunnel and then moved to different locations in the nozzle to change the Mach number. At each Mach number, the value of ρu was changed while recording the voltage E.

The term $\partial \ln E/\partial \phi$ required for Δe_v was also obtained by direct calibration. This was accomplished by mounting the wire on the tunnel centre-line and varying the angle of incidence of the probe holder to vary ϕ while recording E.

The value of $\partial \ln E/\partial \ln T_t$ could not be established with sufficient accuracy by a direct calibration procedure, so Δe_{T_t} was determined by means of (6*b*) using the following substitutions (Morkovin 1956):

$$\left\{\frac{\partial \ln Nu_t}{\partial \ln \theta} + \frac{\theta}{\theta - \eta}\right\} = 2K\left[\frac{\partial \ln E}{\partial \ln R_w} + \left(\frac{1}{2} - \frac{R_w}{R_w + R_s}\right)\right],$$

$$n_t = 0{\cdot}885, \quad m_t = 0{\cdot}765,$$

R_w being the wire resistance and R_s the series resistance in the anemometer bridge, and with $\Delta e_{\rho u}$ taken from the direct calibration discussed above. The value of $\partial \ln E/\partial \ln R_w$ was obtained from a curve fit of the data taken at the time of the fluctuating measurements. K is simply the slope of $\ln R_w$ *vs.* $\ln T_w$ $(\partial \ln R_w/\partial \ln T_w)$.

The resulting set of sensitivities is thus obtained from quantities that are either calibrated *in situ*, calibrated beforehand or are known physical properties of air and tungsten.

To obtain the turbulent Reynolds stress and heat-transfer terms, we examine the mean square of the fluctuating voltage [equation (5)] from the yawed wire:

$$\overline{E'^2} = \overline{\left[\Delta e_{\rho u}\frac{100(\rho u)'}{\overline{\rho u}} + \Delta e_{T_t}\frac{100T_t'}{\overline{T}_t} \pm \Delta e_v \frac{100v'}{\overline{u}}\right]^2}$$

$$= (\Delta e_{\rho u})^2 \frac{\overline{(\rho u)'^2}}{(\overline{\rho u})^2} \times 10^4 + (\Delta e_{T_t})^2 \frac{\overline{T_t'^2}}{\overline{T}_t^2} \times 10^4 + (\Delta e_v)^2 \frac{\overline{v'^2}}{\overline{u}^2} \times 10^4$$

$$+ 2\Delta e_{\rho u}\Delta e_{T_t}\frac{\overline{(\rho u)'T_t'}}{\overline{\rho u}\overline{T}_t} \times 10^4 \pm 2\Delta e_{T_t}\Delta e_v \frac{\overline{T_t'v'}}{\overline{T}_t\overline{u}} \times 10^4 \pm 2\Delta e_{\rho u}\Delta e_v \frac{\overline{(\rho u)'v'}}{\overline{\rho u}\overline{u}} \times 10^4.$$

Mean-square readings were taken before and after the hot-wire sensor was rotated through 180° about its axis. Then, taking the difference of these readings, we have

$$\overline{E_0'^2} - \overline{E_{180}'^2} = 4\left[\Delta e_{T_t}\Delta e_v \frac{\overline{T_t'v'}}{\overline{T}_t\overline{u}} + \Delta e_{\rho u}\Delta e_v \frac{\overline{(\rho u)'v'}}{\overline{\rho u}\overline{u}}\right] \times 10^4,$$

which may be written as

$$\frac{\overline{E_0'^2} - \overline{E_{180}'^2}}{4\Delta e_v \Delta e_{T_t} \times 10^4} = \frac{\overline{T_t'v'}}{\overline{T}_t\overline{u}} - r\frac{\overline{(\rho u)'v'}}{\overline{\rho u}\overline{u}},$$

where $r = -\Delta e_{\rho u}/\Delta e_{T_t}$. The ratio r changes with the wire overheat ratio

$$a_w \equiv (R_w - R_r)/R_r,$$

so that the above equation may be solved for the physical variables if data are obtained for at least two overheat ratios. In this study, four overheat ratios were used and a least-squares technique was used to solve for $\overline{(\rho u)'v'}/\overline{\rho u}^2$ and $\overline{T_t'v'}/\overline{T}_t\overline{u}$ from the resulting overdetermined system of simultaneous equations. These two terms may be expressed in terms of $\overline{u'v'}$ and $\overline{v'T'}$ by writing them as

$$\frac{\overline{T_t'v'}}{\overline{T}_t\overline{u}} = \alpha\frac{\overline{v'T'}}{\overline{u}\overline{T}} + \beta\frac{\overline{u'v'}}{\overline{u}^2},$$

$$\frac{\overline{(\rho u)'v'}}{\overline{\rho u}^2} = \frac{\overline{u'v'}}{\overline{u}^2} - \frac{\overline{v'T'}}{\overline{u}\overline{T}},$$

where $\alpha = 1/[1 + \frac{1}{2}(\gamma - 1)M^2]$ and $\beta = (\gamma - 1)M^2\alpha$. Solving for $\overline{v'T'}$ and $\overline{u'v'}$ from the above, we have

$$\overline{v'T'} = \overline{u}\overline{T}\left[\frac{1}{\alpha+\beta}\frac{\overline{T_t'v'}}{\overline{T}_t\overline{u}} - \frac{\beta}{\alpha+\beta}\frac{\overline{(\rho u)'v'}}{\overline{\rho u}^2}\right],$$

$$\overline{u'v'} = \overline{u}^2\left[\frac{1}{\alpha+\beta}\frac{\overline{T_t'v'}}{\overline{T}_t\overline{u}} + \frac{\alpha}{\alpha+\beta}\frac{\overline{(\rho u)'v'}}{\overline{\rho u}^2}\right].$$

4. Results and discussion

The results of interest in this investigation are shown in graphical form in figures 5–8.

The wall surface static-pressure distribution throughout the interaction region

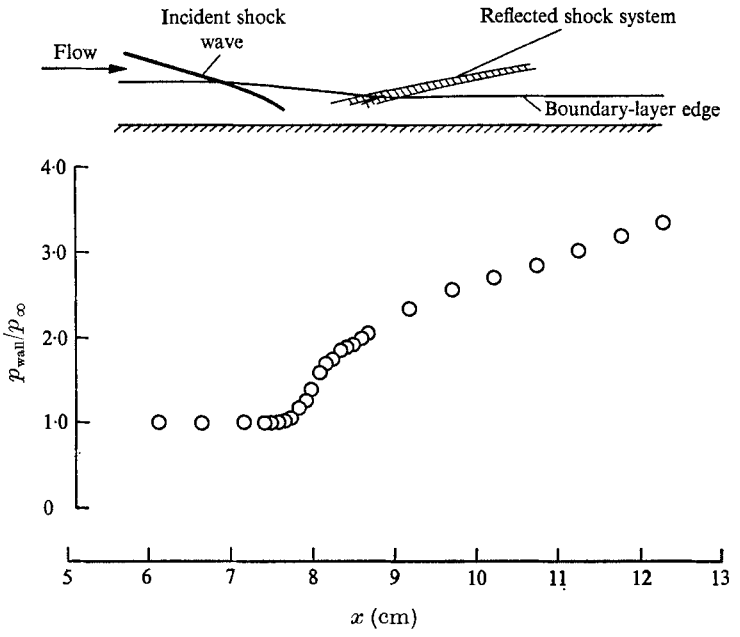

FIGURE 5. Surface static pressures. p_∞ is a free-stream pressure.

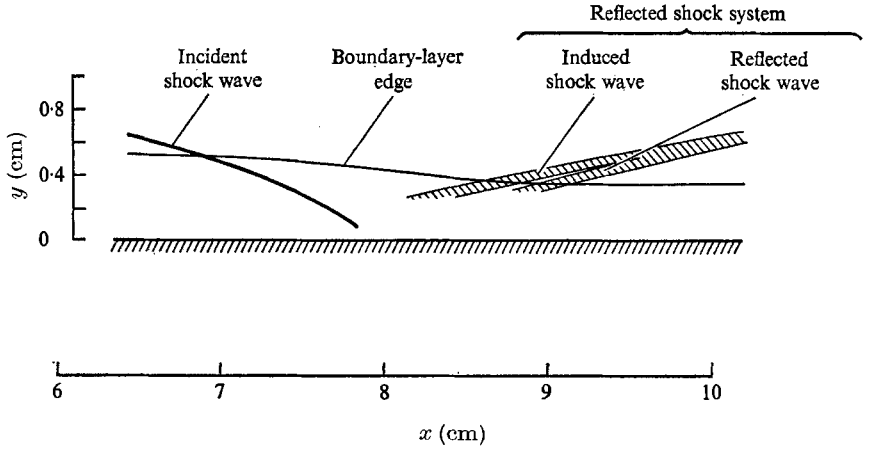

FIGURE 6. Experimentally deduced flow field.

is shown in the lower portion of figure 5. Mean-flow results obtained from Pitot pressures and total-temperature data combined with calculated static pressures (Rose 1970) yield the general flow-field information shown in the upper portion of figure 5. A detailed view of the experimentally deduced flow field in the immediate vicinity of the incident and reflected shock waves is shown in figure 6. The indicated boundary-layer edge is based on total-temperature profiles. Profiles of mean velocity, density and static temperature at five streamwise stations upstream, within and downstream of the interaction region are shown in figure 7.

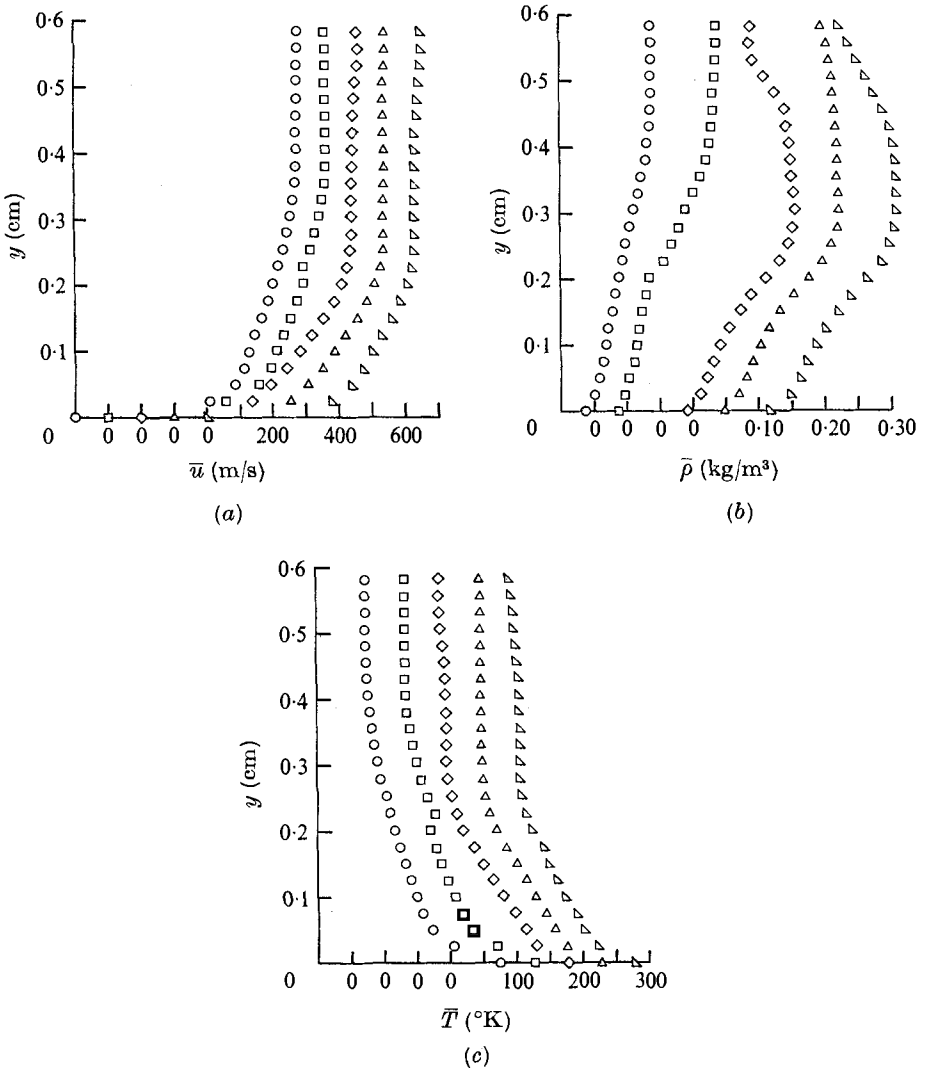

FIGURE 7. Mean flow. (*a*) $\bar{u}$, (*b*) $\bar{\rho}$, (*c*) $\bar{T}$.

	○	□	◇	△	◺
Station (cm)	6·10	7·62	9·65	10·16	11·68

These mean-flow results will not be discussed in detail since they are similar to previously reported information on interactions between turbulent boundary layers and shock waves. They are presented here since they define the flow in which the fluctuating-flow data were obtained.

The fluctuating-flow data ($\bar{\rho}\overline{u'v'}$ and $\bar{\rho}\overline{v'T'}$) are shown in figure 8 for the same five streamwise stations as in figure 7. The values at the wall ($y = 0$) are assumed to be zero. Both $\bar{\rho}\overline{u'v'}$ and $\rho\overline{v'T'}$ fall to zero essentially beyond the boundary-layer edge in agreement with similar data obtained in incompressible flows. The data are presented in a form that includes the effect of the mean density $\bar{\rho}$,

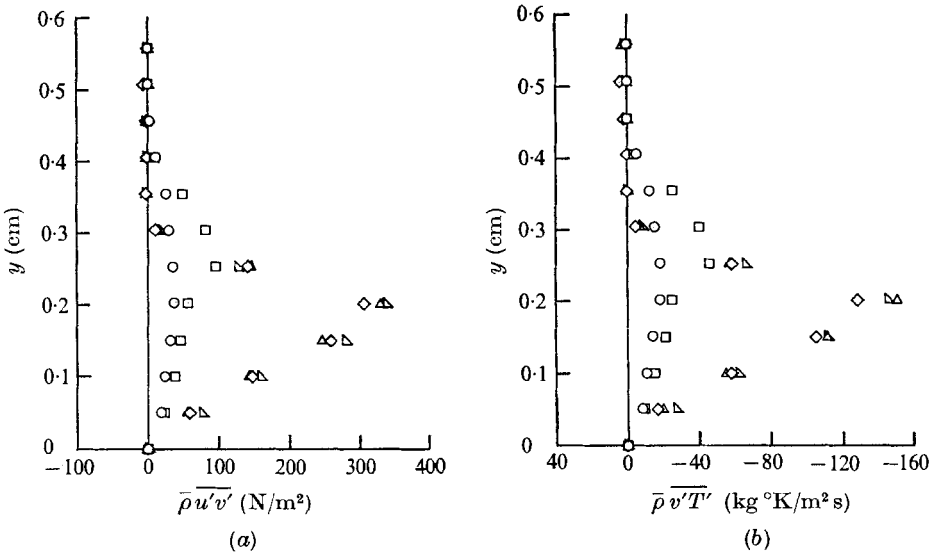

FIGURE 8. Fluctuating flow. (*a*) $\bar{\rho}\,\overline{u'v'}$, (*b*) $\bar{\rho}\,\overline{v'T'}$. Symbols as in figure 7.

which is consistent with the form of the fluctuating terms appearing in the conservation equations (2*a*) and (3). The inclusion of the mean density tends to shift the maxima in both $\bar{\rho}\,\overline{u'v'}$ and $\bar{\rho}\,\overline{v'T'}$ away from the wall (where the maxima occur in incompressible flows). These maxima near the middle of the boundary layer are accentuated in the flow downstream of the immediate interaction region. This is consistent with the observed behaviour of incompressible boundary layers in adverse pressure gradients (e.g. Sandborn & Slogar 1955).

Further comparison of the levels of $\bar{\rho}\,\overline{u'v'}$ and $\bar{\rho}\,\overline{v'T'}$ upstream and downstream of the interaction indicates that the interaction significantly alters the mixing characteristics of the boundary layer. Near the centre of the layer, the downstream levels are approximately an order of magnitude larger than those observed upstream. Furthermore, these increased levels persist as far downstream of the interaction as data were obtained. A manifestation of the increased mixing rates is seen from additional mean-flow information shown in figure 9. The mass flow in the boundary layer relative to its initial value is shown throughout the interaction. It is clear that the rate $d\dot{m}/dx$ of mass entrainment is about an order of magnitude greater downstream of the interaction than upstream.

With respect to modelling the observed behaviour of the fluctuating-flow data for use in computer programs, we note the following. The increase in mean density across the interaction accounts for only about one quarter of the increase in $\bar{\rho}\,\overline{u'v'}$ and $\bar{\rho}\,\overline{v'T'}$. Thus, actual increases in $\overline{u'v'}$ and $\overline{v'T'}$ by about a factor of 4 are evident from the data.

It is clear from the data presented in figure 7(*a*) that an increase in $\partial\bar{u}/\partial y$ of only about a factor of 2 occurs across the interaction. Thus, it would be unlikely that one could explain the fourfold increase in $\overline{u'v'}$ on the basis of an equilibrium shear-stress model that directly relates $\overline{u'v'}$ to $\partial\bar{u}/\partial y$. It is quite probable that sophisticated non-equilibrium descriptions of the turbulent mixing rates such

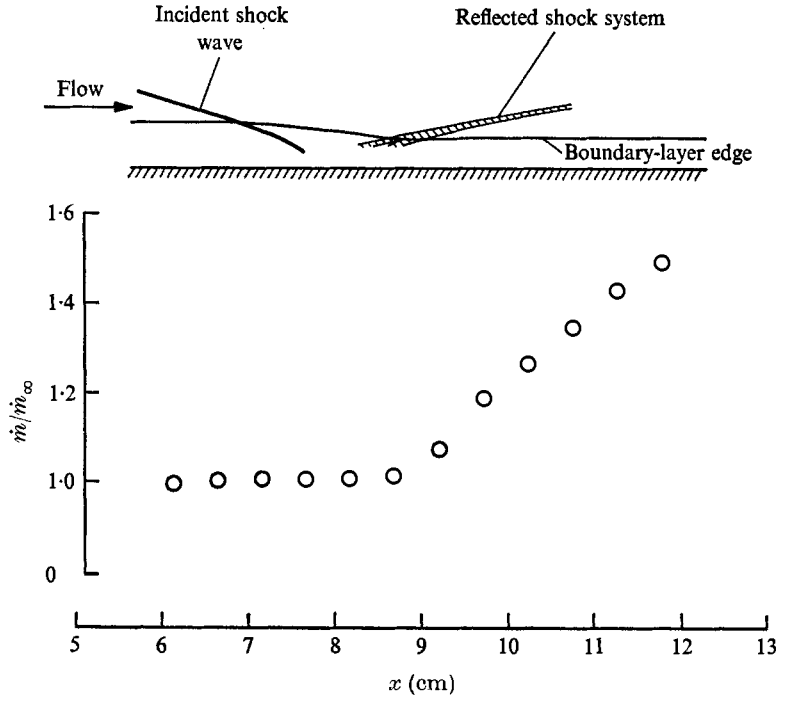

FIGURE 9. Boundary-layer mass flow throughout interaction. $\dot{m}_\infty$ is upstream value.

as those suggested by Bradshaw & Ferriss (1971) or Donaldson (1972) will be required to describe these flows. This is true even far downstream of the interaction since the shear stress has not begun to 'relax' to its equilibrium value, at least, as far downstream as data were obtained.

The accuracy of the data is estimated to be $\pm 3\%$ and $\pm 15\%$ of the values shown for the mean-flow information and fluctuating-flow information, respectively (Rose 1972). These uncertainties should be borne in mind when viewing the data; however, they are not so large as to invalidate the conclusions that can be drawn from the above discussion.

5. Conclusions

Mean- and fluctuating-flow data have been given for a turbulent boundary layer in a shock-wave-induced pressure gradient. The results indicate that some of the features of the turbulent shear stress are similar to those found in incompressible flows with adverse pressure gradients. The turbulent mixing rates (shear stress and heat transfer) are substantially increased as a result of the shock-wave/boundary-layer interaction. These increases cannot be accounted for with an equilibrium model of turbulence, but probably must be described by non-equilibrium models. Furthermore, it is shown that the non-equilibrium effects persist far downstream of the interaction region.

REFERENCES

BRADSHAW, P. & FERRISS, D. H. 1971 Calculation of boundary-layer development using the turbulent energy equation: compressible flow on adiabatic walls. *J. Fluid Mech.* **46**, 83–110.

DONALDSON, C. DUP. 1972 Calculation of turbulent shear flows for atmospheric and vortex motions. *A.I.A.A. J.* **10**, 4–12.

KISTLER, A. L. 1959 Fluctuation measurements in a supersonic turbulent boundary layer. *Phys. Fluids*, **2**, 290–296.

LAUFER, J. 1961 Aerodynamic noise in supersonic wind tunnels. *J. Aero. Sci.* **28**, 685–692.

MORKOVIN, M. V. 1956 Fluctuations and hot-wire anemometry in compressible fluids. *AGARDograph*, no. 24.

MORKOVIN, M. V. & PHINNEY, R. E. 1958 Extended applications of hot-wire anemometry to high-speed turbulent boundary layers. *Johns Hopkins University, Dept. Aeron. Rep.* AFOSR TN-58-469.

ROSE, W. C. 1970 A method for analyzing the interaction of an oblique shock wave with a boundary layer. *N.A.S.A. Tech. Note*, D-6038.

ROSE, W. C. 1972 The behaviour of a compressible turbulent boundary layer in a shock-wave induced adverse pressure gradient. Ph.D. thesis, University of Washington. (See also *N.A.S.A. Tech. Note*, D-7092.)

SANDBORN, V. A. & SLOGAR, R. J. 1955 Study of the momentum distribution of turbulent boundary layers in adverse pressure gradients. *N.A.C.A. Tech. Note*, no. 3264.